Current Optics and Photonics
Vol. 1, No. 5, October 2017, pp. 440-455

ISSN: 2508-7266(Print) / ISSN: 2508-7274(Online)
DOI: https://doi.org/10.3807/COPP.2017.1.5.440

Performance Analysis of FSO Communication Systems with Photodetector Multiplexing

Jianfeng Feng and Xiaohui Zhao*

College of Communication Engineering, Jilin University, Changchun 130000, Jilin, China

(Received January 10, 2017 : revised June 15, 2017 : accepted July 18, 2017)

In this paper, we carry out a performance analysis of a two-user free-space optical (FSO) communication system with photodetector multiplexing, in which the two users are defined as the primary user (PU) and secondary user (SU). Unlike common single-user FSO systems, our photodetector multiplexing FSO system deploys a shared detector at the receiver and enables PU and SU to send their own data synchronously. We conduct the performance analysis of this FSO system for two cases: (1) in the absence of background radiation, and (2) in the presence of background radiation. Decision strategies for PU and SU are presented according to the two scenarios above. Exact and approximate conditional symbol-error probability (SEP) expressions for both PU and SU are derived, in an ideal channel with no fading. Average SEP expressions are also presented in the no-background-radiation scenario. Additionally, in some particular cases where the power ratio tends to 0.5 or 1, approximate SEP expressions are also obtained. Finally, numerical simulations are presented under different conditions, to support the performance analysis.

Keywords : Free space optical communication, Performance analysis, Photodetector multiplexing
OCIS codes : (040.5160) Photodetectors; (060.4510) Optical communication; (010.3310) Laser beam transmission

I. INTRODUCTION

Recently, free-space optical (FSO) communication has attracted considerable research attention, since it has many advantages and possible applications. For example, it has been recognized as a promising solution for metropolitan area network (MAN) extension, fiber back-up, backhaul for wireless cellular networks, and disaster recovery [1]. Compared to their radio-frequency (RF) counterparts, FSO links provide several distinguishing properties, such as very high data rates and a large amount of available, license-free frequency spectrum [2]. However, FSO communications are vulnerable to pointing errors and scintillations. These pointing errors coming from misalignment between transmitter and receiver in long-range outdoor applications, and scintillations due to atmospheric turbulence can seriously deteriorate communication performance in FSO systems [3].

To overcome the above disadvantages, many techniques have been applied in FSO systems, such as channel coding [4], spatial diversity [4-17], adaptive transmission [18, 19], relay-assisted (cooperative) transmission [20-22] and hybrid RF/FSO systems [23, 24]. Among these techniques, spatial diversity is commonly used due, to its simple and efficient features. Spatial diversity can be realized via receive diversity at the receiver [4-7], transmit diversity at the transmitter [8, 9], or a combination of the two [10-17]. Aperture averaging and multiple apertures at the receiver are two simple solutions to receive diversity. Fading reduction by aperture-averaging receivers in turbulent FSO systems is discussed in [4]. In [5], the exact expressions for the aperture-averaging factor in the weak-turbulence regime are developed, for both plane and spherical waves. Outage probability and bit-error rate (BER) performance of FSO links with multiple apertures at the receiver are presented in [6] and [7]. In [8], a transmit-diversity scheme combining transmit laser selection (TLS) and space-time trellis code (STTC) is analyzed. In [9], a BER evaluation is presented by means of numerical simulations, to demonstrate the improvement of a multibeam system over its single-beam counterpart.

*Corresponding author: xhzhao@jlu.edu.cn

Color versions of one or more of the figures in this paper are available online.

Symbol-error probability (SEP) for MIMO (Multiple-Input Multiple-Output) FSO transmission with Q-ary PPM (pulse-position modulation) and Multipulse PPM is obtained in [10] and [11] respectively. In [12], error-rate performance of FSO systems for K-distributed atmospheric turbulence channels is investigated. A new power-series-based representation is proposed for the PDF (probability density function) of the Gamma-Gamma fading FSO links with pointing errors in [13], and based on this PDF the performance of FSO MIMO links is analyzed. By the PDF approximation of the sum of the independent and identically distributed Gamma-Gamma random variables (RVs) through the $\alpha-\mu$ distribution, an ergodic capacity characterization of MIMO FSO systems is provided in [14]. Diversity gain and outage probability for MIMO FSO links with misalignment are studied in [15-17].

The current literature for the performance analysis of FSO communication systems mainly concentrates on single-user regular FSO systems. These studies attempt to improve communication performance of FSO systems using traditional RF technologies, such as diversity, relaying, etc. However, FSO communication is a kind of peer-to-peer transmission. In a two-user regular FSO system, at least two independent photodetectors are needed for the two users. Consequently, system cost increases with the number of users. Our aim in this study is to save a set of receiving devices by photodetector multiplexing in a two-user FSO system, and to improve the communication performance.

In this paper we analyze the performance of an FSO communication system with two users. These two FSO users are denoted as the primary user (PU) and secondary user (SU) respectively. We assume PU and SU send their own BPPM (binary pulse-position) modulated data pulses synchronously. The shared detector at the destination node decides on the superposed symbols sent by PU and SU through decision rules. The performance of this FSO communication system is evaluated with the metric of SEP (symbol-error probability). We derive the maximum-likelihood (ML) decision rule in the presence of background radiation, based on multiple-hypothesis testing. Exact conditional analytic expressions of SEP for both PU and SU are presented, in the presence and absence of background radiation. The average SEP expressions are also derived, based on an optical channel in which both atmospheric turbulence and misalignment errors are considered. Furthermore, we also discuss the approximate behavior of this FSO system at high symbol energy, and the corresponding approximate expressions are provided. Numerical simulations are also provided, for more intuitive explanation and presentation.

The remainder of the paper is organized as follows. In Section 2, the model of the two-user FSO system is introduced. Performance analysis without background radiation is provided in Section 3. The ML decision rule and SEP expressions for both PU and SU in the presence of background radiation are derived in Section 4. The exact and asymptotic expressions obtained in the previous sections are numerically evaluated and interpreted in Section 5. Finally, we review our main results and draw some conclusions in Section 6.

II. SYSTEM MODEL

Figure 1 depicts a block diagram of the two-user FSO communication system used in this paper. We define one source node as the primary user (PU), and another one as the secondary user (SU). Total transmitted power of PU and SU is fixed, and is allocated to PU and SU with the condition that PU always has larger transmitted power than SU. Typically we assign the source node with more stringent requirements for communication quality, so that PU can have better communication performance. The laser sources of PU and SU operate at the same wavelength, in order to share optical components at the receiver. We assume that the transmitted symbols from PU and SU can be exactly aligned by the high-precision synchronous signals generated at the synchronization unit. A shared detector is deployed at the destination node, to simultaneously detect the symbols from PU and SU.

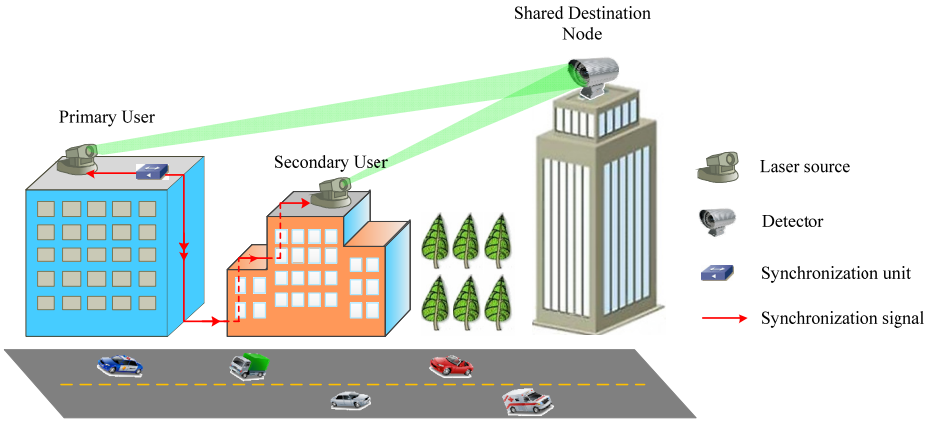

FIG. 1. Two-user FSO communication system.

Next we present specific details and symbol definitions for this two-user FSO system. We define the total transmitted power of PU and SU as $P = P_1 + P_2$, where P_1 and P_2 are the transmitted optical power of PU and SU respectively. P is allocated to PU and SU in a certain proportion, and the power allocated to PU is higher than that to SU, *i.e.* $P_1 > P_2$. Then we define this proportion with a coefficient α, thus the powers of PU and SU can be expressed as $P_1 = \alpha P$ and $P_2 = (1-\alpha)P$. As mentioned above, BPPM (binary pulse-position modulation) is adopted as the modulation format in our FSO communication system. In BPPM, a symbol interval T_s is subdivided into two slots of size T with $T = T_s/2$, and the digital information is sent by the pulse of the laser source in one of the two slots. We define the symbols of PU and SU as $s_{PU}, s_{SU} \in \{1,2\}$ respectively, where 1 means the pulse appears in the first slot, and 2 means it is in the second one. We define the symbol energies of PU and SU at the transmitter as $E_s^{PU} = P_1 T = \alpha PT$ and $E_s^{SU} = P_2 T = (1-\alpha)PT$ respectively.

The optical pulses suffer random fading, due to atmospheric turbulence and misalignment errors, when they go through the optical channel. Hence the optical pulse powers of PU and SU measured at the receiver can be expressed as $P_{1r} = \alpha I_1 P$ and $P_{2r} = (1-\alpha) I_2 P$ respectively, where I_1 and I_2 are the real-valued fading gain (irradiance). We assume I_1 and I_2 are independent and identically distributed, for which the probability density function (PDF) is derived by F. Yang as [25]

$$f_{I'}(I') = \frac{\alpha\beta\varphi^2}{A_0\Gamma(\alpha)\Gamma(\beta)} G_{1,3}^{3,0}\left[\frac{\alpha\beta I'}{A_0}\middle| \begin{matrix}\varphi^2 \\ \varphi^2-1, \alpha-1, \beta-1\end{matrix}\right], \quad I' \geq 0 \tag{1}$$

where $\varphi = \omega_{zeq}/2\sigma_s$, ω_{zeq} is the equivalent beam width and $\omega_{zeq}^2 = \left[\omega_z^2\sqrt{\pi}erf(v)\right]/\left[2v\exp(-v^2)\right]$, ω_z is the beam waist width (a Gaussian beam is assumed), and σ_s^2 is the jitter variance at the receiver. A_0 is calculated using $A_0 = erf(v)^2$ and $v = \sqrt{\pi}r/\sqrt{2}\omega_z$, where r is the aperture radius of the detector and $erf(x)$ is the error function. The remaining two parameters α and β are related to the small- and large-scale turbulence eddies obtained as in [26]

$$\alpha = \left[\exp\left(0.49\sigma_x^2/\left(1+1.11\sigma_x^{12/5}\right)^{7/6}\right)-1\right]^{-1},$$

$$\beta = \left[\exp\left(0.51\sigma_x^2/\left(1+0.69\sigma_x^{12/5}\right)^{5/6}\right)-1\right]^{-1},$$

where σ_x^2 is the log irradiance variance.

$G_{p,q}^{m,n}\left[z\middle| \begin{matrix}a_1,\ldots,a_n,a_{n+1},\ldots,a_p \\ b_1,\ldots,b_m,b_{m+1},\ldots,b_q\end{matrix}\right]$ is Meijer's G-function.

The n^{th} moment of I' is derived in [25]

$$E\left[I'^n\right] = \frac{A_0^n\varphi^2\Gamma(\alpha+n)\Gamma(\beta+n)}{(n+\varphi^2)\Gamma(\alpha)\Gamma(\beta)(\alpha\beta)^n}. \tag{2}$$

Letting $n=1$, we can get the expectation of I' as $I_0 = E[I'] = A_0\varphi^2/(\varphi^2+1)$, which is usually on the order of 10^{-3}. To better show the randomness of the irradiance, we determine the PDF of the normalized irradiance $I = I'/I_0$ as

$$f_I(I) = \frac{\alpha\beta\varphi^4}{(\varphi^2+1)\Gamma(\alpha)\Gamma(\beta)} G_{1,3}^{3,0}\left[\frac{\alpha\beta\varphi^2}{\varphi^2+1} I\middle| \begin{matrix}\varphi^2 \\ \varphi^2-1, \alpha-1, \beta-1\end{matrix}\right], \quad I \geq 0. \tag{3}$$

Using the symbol definitions above, we can evaluate the symbol energy of PU at the receiver through $P_{1r}T = I_1 E_s^{PU}$ and the corresponding symbol energy of SU is $P_{2r}T = I_2 E_s^{SU}$. According to the symbols sent by PU and SU, the wave forms at the receiver are shown in Fig. 2. For data 1 and data 2 in Fig. 2, when PU sends the same data as SU, the two laser pulses at the receiver overlap; if different data are sent, two staggered laser pulses appear at the detector. In Fig. 2(a), the scenario with no background radiation, the total energy of each BPPM symbol is denoted by $I_1 E_s^{PU} + I_2 E_s^{SU}$. For the FSO communication system with background radiation, we assume that the background radiation power P_b is constant in each time slot, and the

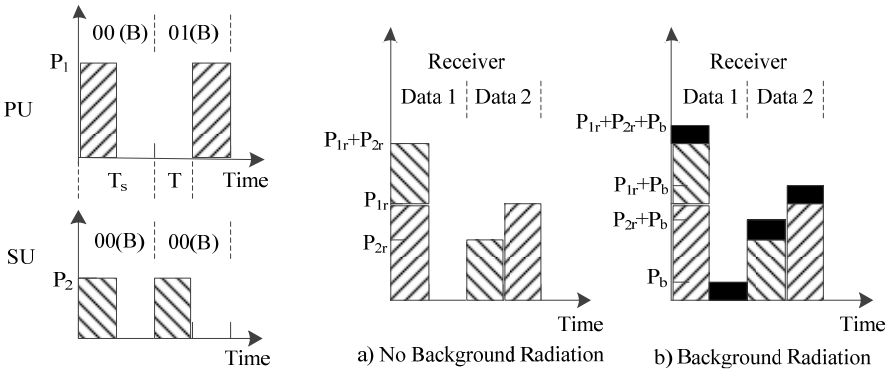

FIG. 2. Waveforms at the receiver.

total symbol energy is calculated by $I_1E_s^{PU}+I_2E_s^{SU}+2P_bT$. If we define the background radiation energy of each slot as $E_b=P_bT$, then $I_1E_s^{PU}+I_2E_s^{SU}+2E_b$.

The optical detection at the receiver can be modeled as a Poissonian point process [10], *i.e.* the number of photoelectrons generated by the incident light in the pulse slot is a Poissonian random variable with parameter λ, where λ is the expectation value of this Poissonian random variable to represent the average photoelectron number in the designated slot. In [27], $\lambda=\eta P_rT/hf$, where P_r is the power of the incident optical signal, η is the quantum efficiency of the photoelectric detector, h is Planck's constant, and f is the frequency of incident light. We define $\lambda_{PU}=\eta P_1T/hf=\eta E_s^{PU}/hf$ corresponding to the transmitted power of PU; then the average photoelectron at the receiver is $\lambda_{PU}I_1$. Similarly, $\lambda_{SU}=\eta P_2T/hf=\eta E_s^{SU}/hf$, and the average number of photoelectrons generated by SU is $\lambda_{SU}I_2$. In the background-radiation scenario, the photoelectrons generated by the background radiation and dark current in each time slot are also modeled as a Poissonian random variable with parameter $\lambda_b=\eta E_b/hf$.

III. PERFORMANCE ANALYSIS WITHOUT BACKGROUND RADIATION

The atmospheric turbulence channel can be modeled as a slowly fading channel, according to the experiment demonstrated in [28], which means that the fading factor is constant over millions of symbols. Hence we can assume that channel-state information is known perfectly at the receiver (PCSIR). In other words, the fading factors I_1 and I_2 are known when the receiver decides the symbols. To represent photoelectron numbers in a designated symbol, we define a two-dimensional vector $\mathbf{Z}=[Z_1,Z_2]$, where Z_1 is the photoelectron number in the first time slot and Z_2 corresponds to the second time slot. If no background radiation is considered, there are two kinds of waveforms at the shared detector. In Fig. 2, we know when PU sends the same symbol as SU, the optical pulses at the receiver overlap and are superimposed; otherwise, the laser pulses are staggered. In the overlap scenario, one of Z_1 and Z_2 is a Poissonian random variable, while the other is definitely zero. Since intensity modulation plus direct detection (IM/DD) is adopted, the parameter of this Poissonian random variable is $\lambda_{PU}I_1+\lambda_{SU}I_2$, *i.e.* $Z_q \quad \pi(\lambda_{PU}I_1+\lambda_{SU}I_2)$, $q=1$ *or* 2. In the staggered case, both Z_1 and Z_2 are Poissonian random variables and the parameters are $\lambda_{PU}I_1$ and $\lambda_{SU}I_2$ respectively. As a matter of routine, z_1 and z_2 are the realizations of the random variable Z_1 and Z_2.

3.1. Decision Strategy

The decision variables of PU and SU are denoted by $\hat{s}_{PU}$ and $\hat{s}_{SU}$ respectively. When background radiation is not considered, the data from SU can be treated as interference for PU. Since the transmitted power of PU is always larger than that of SU, we just select the time slot with more photoelectrons as the data of PU. One exception is when the photoelectron numbers of the two time slots are equal; in this case, PU will make a decision randomly between the two time slots. To summarize, PU decides in favor of $\hat{s}_{PU}$ according to the following strategy:

$$\hat{s}_{PU}=\begin{cases} rand(1,2), & z_1=z_2 \\ \arg\max_{q=1,2} z_q & z_1\neq z_2 \end{cases} \tag{4}$$

The decision strategy for SU is similar to that for PU, but some changes are needed. First, the time slot with fewer photoelectrons cannot always be considered the data of SU. This decision is effective only when PU sends different data than SU, and neither of the two time slots is empty. Second, when PU sends the same data as SU, the optical pulses overlap and one of the two time slots is empty. In this scenario we decide on the nonempty time slot for SU's data. We must note specially that the empty time slot is a *necessary* condition for PU to send the same data as SU, but it is not a *sufficient* condition. If different data are sent, the appearance of an empty time slot is also possible. However, neither of the two time slots being empty definitely means that PU sends different data than SU. To summarize, SU will decide in favor of $\hat{s}_{SU}$ according to the following strategy:

$$\hat{s}_{SU}=\begin{cases} rand(1,2), & z_1=z_2 \\ \arg_q\left[z_q\neq 0\right], & \begin{array}{l}(z_1=0 \ and \ z_2\neq 0) \ or \\ (z_1\neq 0 \ and \ z_2=0)\end{array} \\ \arg\min_{q=1,2} z_q, & z_1\neq z_2\neq 0 \end{cases} \tag{5}$$

3.2. Symbol-error Probability of PU

In this section we evaluate the symbol-error probability (SEP) of PU under the condition of I_1 and I_2, in the case of no background radiation. Therefore, the average SEP of PU is derived based on the channel models in the previous section. Finally, the approximate PU SEP is presented. Based on Eq. (4), we know that the data based on wrong decisions for PU appear in the following cases.

Case A: Random decision

When the photoelectron number of the two time slots is equal, namely $z_1=z_2$, the receiver makes a decision randomly between the two time slots. As a result, the probabilities of correct and incorrect decisions are equal. The random decision can be further divided into the following two categories.

Case A-1: Neither time slot is zero

In this category, $z_1=z_2$ but none of the two time slots are empty, *i.e.* $z_1=z_2\neq 0$. Since there is no background

radiation, the pulses sent by PU and SU are interleaved, which means PU sends different data than SU. This is an implicit condition for case A-1. In brief, case A-1 occurs only when the following two conditions are simultaneously satisfied: (a) different data are sent, and (b) $z_1 = z_2$. In case A-1, one time slot is use by PU's laser pulse and the other by SU's pulse. The photoelectron numbers of the two slots are two Poissonian random variables with parameters $\lambda_{PU} I_1$ and $\lambda_{SU} I_2$ respectively. Then we can calculate the SEP of PU in case A-1 as

$$\begin{aligned} P_s^{PU,A-1}(e \mid I_1, I_2) &= \Pr(e \mid z_1 = z_2 \neq 0) \\ &\quad \Pr(z_1 = z_2 \mid z_1 \neq 0, z_2 \neq 0) \\ &\quad \Pr(z_1 \neq 0, z_2 \neq 0) \\ &= \frac{1}{2}\sum_{k=1}^{\infty} \Pr(Z_1 = k, Z_2 = k) \Pr(s_{PU} \neq s_{SU}) \end{aligned} \tag{6}$$

From [29], we know that X is a Poissonian random variable with parameter λ if X takes the values $0,1,2,...,\infty$, with probability

$$\Pr\{X = k\} = \frac{e^{-\lambda}\lambda^k}{k!}, \quad k = 0,1,2,...,\infty \tag{7}$$

Without loss of generality, we assume that the first time slot is occupied by PU's pulse, and SU's data appear in the second time slot. Therefore, the probability of Z_1 with k photoelectrons is $e^{-\lambda_{PU} I_1}(\lambda_{PU} I_1)^k / k!$. Accordingly, the second time slot has k photoelectrons with a probability of $e^{-\lambda_{SU} I_2}(\lambda_{SU} I_2)^k / k!$. For more concise representation, we define

$$\Theta(k, \lambda) = \Pr\{X = k\} = \frac{e^{-\lambda}\lambda^k}{k!} \tag{8}$$

Then Eq. (6) can be rewritten as

$$\begin{aligned} P_s^{PU,A-1}(e \mid I_1, I_2) &= \frac{1}{4}\sum_{k=1}^{\infty} \frac{e^{-\lambda_{PU} I_1}(\lambda_{PU} I_1)^k}{k!} \frac{e^{-\lambda_{SU} I_2}(\lambda_{SU} I_2)^k}{k!} \\ &= \frac{1}{4}\sum_{k=1}^{\infty} \Theta(k, \lambda_{PU} I_1)\Theta(k, \lambda_{SU} I_1) \end{aligned} \tag{9}$$

Case A-2: Both time slots are zero

This is another scenario where the photoelectron numbers of the two slots are equal, *i.e.* $z_1 = z_2 = 0$. Unfortunately, we cannot judge whether PU and SU send the same or different data in this case. If the same data are sent, one time slot must have zero photoelectrons, and the photoelectron number in the other time slot is a Poissonian random variable with parameter $\lambda_{PU} I_1 + \lambda_{SU} I_2$. Therefore, the probability of $z_1 = z_2 = 0$ under the condition that the same data are sent can be described as

$$\Pr(z_1 = z_2 = 0 \mid s_{PU} = s_{SU}) = \Theta(0, \lambda_{PU} I_1 + \lambda_{SU} I_2) \tag{10}$$

If PU sends different data than SU, the photoelectron numbers of the two time slots are two Poissonian random variables with parameters $\lambda_{PU} I_1$ and $\lambda_{SU} I_2$ respectively. The probability of $z_1 = z_2 = 0$ under the condition of different data being sent can be expressed as

$$\Pr(z_1 = z_2 = 0 \mid s_{PU} \neq s_{SU}) = \Theta(0, \lambda_{PU} I_1)\Theta(0, \lambda_{SU} I_2) \tag{11}$$

Hence we can get the probability of $z_1 = z_2 = 0$ as

$$\begin{aligned} \Pr(z_1 = z_2 = 0) &= \Pr(z_1 = z_2 = 0 \mid s_{PU} = s_{SU}) \Pr(s_{PU} = s_{SU}) \\ &\quad + \Pr(z_1 = z_2 = 0 \mid s_{PU} \neq s_{SU}) \Pr(s_{PU} \neq s_{SU}) \\ &= \Theta(0, \lambda_{PU} I_1 + \lambda_{SU} I_2) \end{aligned} \tag{12}$$

Here the property $\Theta(0, \lambda_{PU} I_1 + \lambda_{SU} I_2) = \Theta(0, \lambda_{PU} I_1) \times \Theta(0, \lambda_{SU} I_2)$ is used. Finally, we can obtain the conditional SEP of PU in case A-2 as

$$\begin{aligned} P_s^{PU,A-2}(e \mid I_1, I_2) &= \Pr(e \mid z_1 = z_2 = 0)\Pr(z_1 = z_2 = 0) \\ &= \frac{1}{2}\Theta(0, \lambda_{PU} I_1 + \lambda_{SU} I_2) \end{aligned} \tag{13}$$

Case B: Nonrandom decision

In this case $z_1 \neq z_2$, and the wrong decision occurs when the time slot with more photoelectrons is not used for the laser pulse sent by PU. This scenario occurs only when PU sends different data than SU, which in fact is also an implicit condition. If the same data are sent and the time slot with overlapping pulses is not empty, it is impossible for PU to make the wrong decision. Without loss of generality, we assume $s_{PU} = 1$, and $s_{SU} = 2$. Since the transmitted power of PU is larger than that of SU, in the first time slot there are more photoelectrons than in the second, and the photoelectron numbers in the two time slots are random variables. It is clear that the wrong decision occurs when $z_1 < z_2$, which implies $Z_1 \sim \pi(\lambda_{PU} I_1)$, and $Z_2 \sim \pi(\lambda_{SU} I_2)$. Therefore, the conditional SEP of PU in case B is the probability of the Poissonian random variable with parameter $\lambda_{PU} I_1$, which is smaller than that of the Poissonian random variable with parameter $\lambda_{SU} I_2$. Then the conditional SEP of PU in case B can be expressed as

$$\begin{aligned} P_s^{PU,B}(e \mid I_1, I_2) &= \sum_{i=1}^{\infty}\sum_{j=0}^{i-1} \Pr(Z_2 = i, Z_1 = j) \Pr(s_{PU} \neq s_{SU}) \\ &= \frac{1}{2}\sum_{i=1}^{\infty}\sum_{j=0}^{i-1} \Theta(i, \lambda_{SU} I_2)\Theta(j, \lambda_{PU} I_1) \end{aligned} \tag{14}$$

We need to point out that the above three cases A-1, A-2, and B are mutually exclusive, so that the conditional SEP of PU with no background radiation can be evaluated as

$$\begin{aligned} P_s^{PU}\left(e\,|\,I_1,I_2\right) &= P_s^{PU,A-1}+P_s^{PU,A-2}+P_s^{PU,B} \\ &= \frac{1}{2}\Bigg[\frac{1}{2}\sum_{k=1}^{\infty}\Theta\left(k,\lambda_{PU}I_1\right)\Theta\left(k,\lambda_{SU}I_2\right) \\ &\quad +\sum_{i=1}^{\infty}\sum_{j=0}^{i-1}\Theta\left(i,\lambda_{SU}I_2\right)\Theta\left(j,\lambda_{PU}I_1\right) \\ &\quad +\Theta\left(0,\lambda_{PU}I_1+\lambda_{SU}I_2\right)\Bigg]. \end{aligned} \tag{15}$$

The average SEP of PU can be obtained by taking the expectation value of the conditional SEP $P_s^{PU}\left(e\,|\,I_1,I_2\right)$ over I_1 and I_2. Since I_1 and I_2 are independent and identically distributed, the average SEP of PU can be expressed as

$$\begin{aligned} P_s^{PU} &= \frac{1}{4}\sum_{k=1}^{\infty}E_{I_1}\left[\Theta\left(k,\lambda_{PU}I_1\right)\right]E_{I_2}\left[\Theta\left(k,\lambda_{SU}I_2\right)\right] \\ &\quad +\frac{1}{2}\sum_{i=1}^{\infty}\sum_{j=0}^{i-1}E_{I_2}\left[\Theta\left(i,\lambda_{SU}I_2\right)\right]E_{I_1}\left[\Theta\left(j,\lambda_{PU}I_1\right)\right] \\ &\quad +\frac{1}{2}E_{I_1}\left[\Theta\left(0,\lambda_{PU}I_1\right)\right]E_{I_2}\left[\Theta\left(0,\lambda_{SU}I_2\right)\right]. \end{aligned} \tag{16}$$

The expectation value $E_{I_1}\left[\Theta\left(k,\lambda_{PU}I_1\right)\right]$ can be evaluated as

$$E_{I_1}\left[\Theta\left(k,\lambda_{PU}I_1\right)\right]=\int_0^{\infty}\frac{e^{-\lambda_{PU}I_1}\left(\lambda_{PU}I_1\right)^k}{k!}f_{I_1}\left(I_1\right)dI_1. \tag{17}$$

Substituting Eq. (3) into Eq. (17), we have

$$\begin{aligned} E_{I_1}\left[\Theta\left(k,\lambda_{PU}I_1\right)\right] &= \frac{\alpha\beta\varphi^4\lambda_{PU}^k}{\left(\varphi^2+1\right)\Gamma\left(\alpha\right)\Gamma\left(\beta\right)k!}\int_0^{\infty}I_1^k e^{-\lambda_{PU}I_1} \\ &\quad G_{1,3}^{3,0}\left[\frac{\alpha\beta\varphi^2 I_1}{\varphi^2+1}\middle|\begin{matrix}\varphi^2\\ \varphi^2-1,\alpha-1,\beta-1\end{matrix}\right]dI_1. \end{aligned} \tag{18}$$

Using Eq. (11) and in [30], the exponential function can be written in the form of Meijer's *G*-function, *i.e.*

$$\exp(-x)=G_{0,1}^{1,0}\left[x\middle|\begin{matrix}-\\ 0\end{matrix}\right]. \tag{19}$$

Substituting Eq. (19) into Eq. (18) and using Eq. (07.34.21.0011.01) in [31] to calculate Meijer's integral from two *G*-functions, after some mathematical development we have

$$\begin{aligned} E_{I_1}\left[\Theta\left(k,\lambda_{PU}I_1\right)\right] &= \frac{\alpha\beta\varphi^4}{\left(\varphi^2+1\right)\Gamma\left(\alpha\right)\Gamma\left(\beta\right)k!\lambda_{PU}} \\ &\quad G_{2,3}^{3,1}\left[\frac{\alpha\beta\varphi^2}{\left(\varphi^2+1\right)\lambda_{PU}}\middle|\begin{matrix}-k,\varphi^2\\ \varphi^2-1,\alpha-1,\beta-1\end{matrix}\right]. \end{aligned} \tag{20}$$

The above expression can be further simplified by Eq. (07.34.16.0001.01) in [31]

$$\begin{aligned} E_{I_1}\left[\Theta\left(k,\lambda_{PU}I_1\right)\right] &= \frac{\varphi^2}{\Gamma\left(\alpha\right)\Gamma\left(\beta\right)k!} \\ &\quad G_{2,3}^{3,1}\left[\frac{\alpha\beta\varphi^2}{\left(\varphi^2+1\right)\lambda_{PU}}\middle|\begin{matrix}1-k,\varphi^2+1\\ \varphi^2,\alpha,\beta\end{matrix}\right]. \end{aligned} \tag{21}$$

We use $\Xi\left(k,\lambda_{PU}\right)$ to represent $E_{I_1}\left[\Theta\left(k,\lambda_{PU}I_1\right)\right]$, and the average SEP of PU can be given as

$$\begin{aligned} P_s^{PU} &= \frac{1}{2}\Bigg[\frac{1}{2}\sum_{k=1}^{\infty}\Xi\left(k,\lambda_{PU}\right)\Xi\left(k,\lambda_{SU}\right) \\ &\quad +\sum_{i=1}^{\infty}\sum_{j=0}^{i-1}\Xi\left(i,\lambda_{SU}\right)\Xi\left(j,\lambda_{PU}\right) \\ &\quad +\Xi\left(0,\lambda_{PU}+\lambda_{SU}\right)\Bigg]. \end{aligned} \tag{22}$$

Under ideal no-fading conditions, I_1 and I_2 are assumed to be unity, and the SEP of PU is $\frac{1}{4}\sum_{k=1}^{\infty}\Theta\left(k,\lambda_{PU}\right)\Theta\left(k,\lambda_{SU}\right)+\frac{1}{2}\sum_{i=1}^{\infty}\sum_{j=0}^{i-1}\Theta\left(i,\lambda_{SU}\right)\Theta\left(j,\lambda_{PU}\right)+\frac{1}{2}\Theta\left(0,\lambda_{PU}+\lambda_{SU}\right)$. Since $\lambda_{PU}+\lambda_{SU}$ is equal to $\eta E_s/hf$, and for an FSO communication system the total symbol energy is usually large enough to ensure $e^{-\lambda_{PU}-\lambda_{SU}}$ approaches zero, we obtain the approximate SEP expression of PU under ideal conditions as

$$\begin{aligned} P_s^{PU,Appro} &\approx \frac{1}{4}\sum_{k=1}^{\infty}\Theta\left(k,\lambda_{PU}\right)\Theta\left(k,\lambda_{SU}\right) \\ &\quad +\frac{1}{2}\sum_{i=1}^{\infty}\sum_{j=0}^{i-1}\Theta\left(i,\lambda_{SU}\right)\Theta\left(j,\lambda_{PU}\right). \end{aligned} \tag{23}$$

Under fading conditions, the approximate average SEP of PU is

$$\begin{aligned} P_s^{PU,Appro} &\approx \frac{1}{4}\sum_{k=1}^{\infty}\Xi\left(k,\lambda_{PU}\right)\Xi\left(k,\lambda_{SU}\right) \\ &\quad +\frac{1}{2}\sum_{i=1}^{\infty}\sum_{j=0}^{i-1}\Xi\left(i,\lambda_{SU}\right)\Xi\left(j,\lambda_{PU}\right). \end{aligned} \tag{24}$$

We will verify this expression in the simulation section.

3.3. Symbol-error Probability of SU

The receiver decides SU data based on the strategy from Eq. (5). Decision error occurs in the following cases.

Case A: Random decision

When the two time slots have the same number of photoelectrons, both PU and SU have a fifty percent probability to make the right decision, and the probability of $z_1 = z_2$ is the same for PU and SU. Thus the conditional SEP of SU due to a random decision is equal to that of PU, and we have

$$P_s^{SU,A}\left(e \mid I_1, I_2\right) = P_s^{PU,A-1}\left(e \mid I_1, I_2\right) + P_s^{PU,A-2}\left(e \mid I_1, I_2\right) \tag{25}$$

Case B: Nonrandom decision

Unlike the decision of PU when $z_1 \neq z_2$, which just selects the time slot with more photoelectrons, the decision of SU is more complex and can be divided into the following sub-cases.

Case B-1: Neither time slot is zero

In this sub-case, neither of the two time slots is empty and the two slots have different photoelectron counts. Hence the evaluation of conditional SEP is similar to that for $P_s^{PU,B}\left(e \mid I_1, I_2\right)$, but the minimum photoelectron numbers of these slots are 1 and 2 respectively. Thus we can describe this conditional SEP of SU in case B-1 as

$$\begin{aligned} P_s^{SU,B-1}\left(e \mid I_1, I_2\right) &= \sum_{i=2}^{\infty}\sum_{j=1}^{i-1} \Pr\left(Z_2 = i, Z_1 = j\right) \Pr\left(s_{PU} \neq s_{SU}\right) \\ &= \frac{1}{2}\sum_{i=2}^{\infty}\sum_{j=1}^{i-1} \Theta\left(i, \lambda_{SU} I_2\right)\Theta\left(j, \lambda_{PU} I_1\right). \end{aligned} \tag{26}$$

Case B-2: Exactly one slot is zero

If only one of the two time slots is empty and PU sends the same data as SU, there will be no wrong decision for SU. A decision error can only occur when different data are sent. For example, we assume PU sends symbol 1, and SU sends 2. If the time slot of SU is empty and the time slot of PU is not empty, the receiver will decide the data of SU as symbol 2, which in fact is wrong. Therefore, the conditional SEP of SU in case B-2 can be expressed as

$$\begin{aligned} P_s^{SU,B-2}\left(e \mid I_1, I_2\right) &= \Pr\left(PU\text{'s slot} \neq 0, SU\text{'s slot} = 0\right) \\ &\quad \Pr\left(s_{PU} \neq s_{SU}\right) \\ &= \frac{1}{2}\Theta\left(0, \lambda_{SU} I_2\right)\left[1 - \Theta\left(0, \lambda_{PU} I_1\right)\right]. \end{aligned} \tag{27}$$

Finally, the conditional SEP of SU is

$$\begin{aligned} P_s^{SU}\left(e \mid I_1, I_2\right) = \frac{1}{2}\Bigg[& \frac{1}{2}\sum_{k=1}^{\infty}\Theta\left(k, \lambda_{PU} I_1\right)\Theta\left(k, \lambda_{SU} I_2\right) \\ & + \sum_{i=2}^{\infty}\sum_{j=1}^{i-1}\Theta\left(i, \lambda_{SU} I_2\right)\Theta\left(j, \lambda_{PU} I_1\right) \\ & + \Theta\left(0, \lambda_{SU} I_2\right)\Bigg]. \end{aligned} \tag{28}$$

As for PU, taking the expectation value of conditional SEP $P_s^{SU}\left(e \mid I_1, I_2\right)$, we can also obtain the average SEP of SU as

$$\begin{aligned} P_s^{SU} = \frac{1}{2}\Bigg[& \frac{1}{2}\sum_{k=1}^{\infty}\Xi\left(k, \lambda_{PU}\right)\Xi\left(k, \lambda_{SU}\right) \\ & + \sum_{i=2}^{\infty}\sum_{j=1}^{i-1}\Xi\left(i, \lambda_{SU}\right)\Xi\left(j, \lambda_{PU}\right) + \Xi\left(0, \lambda_{SU}\right)\Bigg]. \end{aligned} \tag{29}$$

To get an approximate expression for the SEP of SU under ideal no-fading conditions, we first set I_1 and I_2 be 1, then consider the last item $\Theta\left(0, \lambda_{SU}\right)$ in Eq. (28). If PU occupies the majority of the total transmitted power, *i.e.* $\alpha \to 1$, the transmitted power of SU is much smaller than that of PU. Consequently, the average photoelectron number λ_{SU} is small, and the value of P_s^{SU} is dominated by $\Theta\left(0, \lambda_{SU}\right)$. Instead, if $\alpha \to 0.5$, the value of λ_{SU} is slightly smaller than that of λ_{PU}. The last item $\Theta\left(0, \lambda_{SU}\right)$ is no longer a dominant item and can be omitted. Finally, we can get the approximate expression for the SEP of SU as

$$\begin{aligned} P_s^{SU,Appro,\alpha\to 0.5} \approx & \frac{1}{4}\sum_{k=1}^{\infty}\Theta\left(k, \lambda_{PU}\right)\Theta\left(k, \lambda_{SU}\right) \\ & + \frac{1}{2}\sum_{i=2}^{\infty}\sum_{j=1}^{i-1}\Theta\left(i, \lambda_{SU}\right)\Theta\left(j, \lambda_{PU}\right) \end{aligned} \tag{30a}$$

$$P_s^{SU,Appro,\alpha\to 1} \approx \frac{1}{2}\Theta\left(0, \lambda_{SU}\right) + \frac{1}{2}\sum_{i=2}^{\infty}\sum_{j=1}^{i-1}\Theta\left(i, \lambda_{SU}\right)\Theta\left(j, \lambda_{PU}\right) \tag{30b}$$

Similarly, the approximate average SEP for SU in the fading case is

$$\begin{aligned} P_s^{SU,Appro,\alpha\to 0.5} \approx & \frac{1}{4}\sum_{k=1}^{\infty}\Xi\left(k, \lambda_{PU}\right)\Xi\left(k, \lambda_{SU}\right) \\ & + \frac{1}{2}\sum_{i=2}^{\infty}\sum_{j=1}^{i-1}\Xi\left(i, \lambda_{SU}\right)\Xi\left(j, \lambda_{PU}\right) \end{aligned} \tag{31a}$$

$$P_s^{SU,Appro,\alpha\to 1} \approx \frac{1}{2}\Xi\left(0, \lambda_{SU}\right) + \frac{1}{2}\sum_{i=2}^{\infty}\sum_{j=1}^{i-1}\Xi\left(i, \lambda_{SU}\right)\Xi\left(j, \lambda_{PU}\right) \tag{31b}$$

IV. PERFORMANCE ANALYSIS WITH BACKGROUND RADIATION

4.1. Decision Strategy

In practical FSO communication systems, background radiation cannot be removed completely. The number of photoelectrons generated by background radiation is also modeled as a Poissonian random variable with parameter $\lambda_b = \eta E_b / hf$, where E_b is the symbol energy of the background radiation. In the background-radiation scenario, even if the same data are sent and the signal pulses of PU and SU are superimposed in one time slot, photoelectrons may still appear in the other time slot. This is totally different from the scenario without background radiation, in which one of two time slots is definitely empty when the same data are sent. When we take the background radiation into consideration, the photoelectron number of each time slot in a symbol is two Poissonian random variables. According to the data sent by PU and SU, we have the following four hypotheses:

$$\begin{aligned} &H_0 : s_{PU} = 1, s_{SU} = 1 \\ &H_1 : s_{PU} = 1, s_{SU} = 2 \\ &H_2 : s_{PU} = 2, s_{SU} = 1 \\ &H_3 : s_{PU} = 2, s_{SU} = 2 \end{aligned} \tag{32}$$

We define a two-dimensional vector $\mathbf{Z} = [Z_1, Z_2]$ in which the two elements represent the photoelectron numbers in the two time slots respectively. Z_1 and Z_2 are independent Poissonian random variables with different parameters. These parameters are determined according to the four hypotheses in Eq. (32). For example, under hypothesis H_0 both of the optical pulses of PU and SU appear in the first time slot, and $Z_1 \quad \pi(\lambda_{PU} I_1 + \lambda_{SU} I_2 + \lambda_b)$. Meanwhile, the second time slot is occupied by the photoelectrons generated by the background radiation, *i.e.* $Z_2 \quad \pi(\lambda_b)$. In the background-radiation scenario, we also assume the CSI is known perfectly by the receiver. Hence the joint probability distribution function of $\mathbf{Z}$ under hypothesis H_0 conditioned on I_1 and I_2 can be expressed as

$$\begin{aligned} p(\mathbf{Z} \mid H_0, I_1, I_2) &= p(z_1 \mid H_0, I_1, I_2)\, p(z_2 \mid H_0, I_1, I_2) \\ &= \Theta(z_1, \lambda_{PU} I_1 + \lambda_{SU} I_2 + \lambda_b)\, \Theta(z_2, \lambda_b) \\ &= \frac{e^{-(\lambda_{PU} I_1 + \lambda_{SU} I_2 + 2\lambda_b)} (\lambda_{PU} I_1 + \lambda_{SU} I_2 + \lambda_b)^{z_1} \lambda_b^{z_2}}{z_1! z_2!} \end{aligned} \tag{33}$$

Similarly, we can get the conditional joint probability distribution function of $\mathbf{Z}$ under hypotheses H_1, H_2, and H_3 as

$$\begin{cases} p(\mathbf{Z} \mid H_1, I_1, I_2) = \Theta(z_1, \lambda_{PU} I_1 + \lambda_b)\, \Theta(z_2, \lambda_{SU} I_2 + \lambda_b) \\ p(\mathbf{Z} \mid H_2, I_1, I_2) = \Theta(z_1, \lambda_{SU} I_2 + \lambda_b)\, \Theta(z_2, \lambda_{PU} I_1 + \lambda_b) \\ p(\mathbf{Z} \mid H_3, I_1, I_2) = \Theta(z_1, \lambda_b)\, \Theta(z_2, \lambda_{PU} I_1 + \lambda_{SU} I_2 + \lambda_b) \end{cases} \tag{34}$$

Then the log-likelihood function for $\mathbf{Z}$ can be written as

$$\begin{cases} L(\mathbf{Z} \mid H_0, I_1, I_2) = z_1 \ln(\lambda_{PU} I_1 + \lambda_{SU} I_2 + \lambda_b) + z_2 \ln \lambda_b \\ L(\mathbf{Z} \mid H_1, I_1, I_2) = z_1 \ln(\lambda_{PU} I_1 + \lambda_b) + z_2 \ln(\lambda_{SU} I_2 + \lambda_b) \\ L(\mathbf{Z} \mid H_2, I_1, I_2) = z_1 \ln(\lambda_{SU} I_2 + \lambda_b) + z_2 \ln(\lambda_{PU} I_1 + \lambda_b) \\ L(\mathbf{Z} \mid H_3, I_1, I_2) = z_1 \ln \lambda_b + z_2 \ln(\lambda_{PU} I_1 + \lambda_{SU} I_2 + \lambda_b) \end{cases} \tag{35}$$

From the maximum-likelihood (ML) detection rule, we know if hypothesis H_0 is correct, the following inequality group needs to be established:

$$\begin{cases} L(\mathbf{Z} \mid H_0, I_1, I_2) > L(\mathbf{Z} \mid H_1, I_1, I_2) \\ L(\mathbf{Z} \mid H_0, I_1, I_2) > L(\mathbf{Z} \mid H_2, I_1, I_2) \\ L(\mathbf{Z} \mid H_0, I_1, I_2) > L(\mathbf{Z} \mid H_3, I_1, I_2) \end{cases} \tag{36}$$

Substituting Eq. (35) into Eq. (36), we have

$$\frac{z_1}{z_2} > \max\left\{ \frac{\ln(1 + \lambda_{SU} I_2 / \lambda_b)}{\ln[1 + \lambda_{SU} I_2 / (\lambda_{PU} I_1 + \lambda_b)]}, \frac{\ln(1 + \lambda_{PU} I_1 / \lambda_b)}{\ln[1 + \lambda_{PU} I_1 / (\lambda_{SU} I_2 + \lambda_b)]} \right\} \tag{37}$$

We define

$$\kappa = \max\left\{ \frac{\ln(1 + \lambda_{SU} I_2 / \lambda_b)}{\ln[1 + \lambda_{SU} I_2 / (\lambda_{PU} I_1 + \lambda_b)]}, \frac{\ln(1 + \lambda_{PU} I_1 / \lambda_b)}{\ln[1 + \lambda_{PU} I_1 / (\lambda_{SU} I_2 + \lambda_b)]} \right\},$$

which is greater than one. Then we have

$$\kappa = \begin{cases} \dfrac{\ln(1 + \lambda_{SU} I_2 / \lambda_b)}{\ln[1 + \lambda_{SU} I_2 / (\lambda_{PU} I_1 + \lambda_b)]}, & \lambda_{PU} I_1 \geq \lambda_{SU} I_2 \\ \dfrac{\ln(1 + \lambda_{PU} I_1 / \lambda_b)}{\ln[1 + \lambda_{PU} I_1 / (\lambda_{SU} I_2 + \lambda_b)]}, & \lambda_{PU} I_1 < \lambda_{SU} I_2 \end{cases}. \tag{38}$$

(See Appendix for detailed proof).

Then we can obtain the conditional decision region for H_0 as $R(H_0 \mid I_1, I_2) = \{ z_1 / z_2 \,|\, z_1 / z_2 > \kappa \}$. Repeating the process above, we can obtain the decision regions for H_1, H_2, and H_3 respectively. After some calculations, we have the decision rule in the background-radiation scenario as

$$\left(\hat{s}_{PU},\hat{s}_{SU}\right)=\begin{cases}(1,1) & z_1/z_2>\kappa\\ (1,2) & 1<z_1/z_2<\kappa\\ (2,1) & 1/\kappa<z_1/z_2<1\\ (2,2) & z_1/z_2<1/\kappa\end{cases}. \tag{39}$$

Note that we do not take the boundaries of the decision regions into consideration in the above derivations. Since z_1 and z_2 are discrete random variables, the decisions in the cases of $z_1=\kappa z_2$, $z_1=z_2$, and $z_2=\kappa z_1$ must be handled carefully when the likelihood functions are equal. To simplify the analysis, we assume κ is not an integer; then we can ignore the cases of $z_1=\kappa z_2$ and $z_2=\kappa z_1$, since z_1 and z_2 are integers. When $z_1=z_2$, we adopt the random decision used in the previous section. Finally, we rewrite the decision rule for PU in the background radiation scenario as

$$\hat{s}_{PU}=\begin{cases}rand(1,2), & z_1=z_2\\ \arg\max_{q=1,2} Z_q, & z_1\neq z_2\end{cases}. \tag{40}$$

Accordingly, the decision rule for SU is

$$\hat{s}_{SU}=\begin{cases}1, & z_1/z_2>\kappa \;\; or \;\; 1/\kappa<z_1/z_2<1\\ rand(1,2), & z_1=z_2\\ 2, & 1<z_1/z_2<\kappa \;\; or \;\; z_1/z_2<1/\kappa\end{cases}. \tag{41}$$

4.2. Symbol-error Probability of PU

Comparing Eq. (4) to Eq. (40), we can see that the decision rule for PU in the background-radiation scenario is the same as in the no-background-radiation scenario. If two time slots have the same number of photoelectrons, a random decision occurs; otherwise, both background radiation and SU data are treated as interference with PU. Wrong decisions may happen in the following cases.

Case A: Random decision

According to the data sent by PU and SU, the random-decision case can be further divided into cases A-1 and A-2, corresponding to different data and same data respectively.

Case A-1: Different data sent

When different data are sent, the two laser pulses are staggered. In the time slot for PU data, the number of photoelectrons is a Poissonian random variable with parameter $\lambda_{PU}I_1+\lambda_b$, while in the time slot for SU data the parameter of the Poissonian random variable is $\lambda_{SU}I_2+\lambda_b$. The conditional SEP in this case is

$$\begin{aligned}P_s^{PU,A-1,BR}\left(e\,|\,I_1,I_2\right)&=\frac{1}{2}\sum_{k=0}^{\infty}\Pr\left(Z_1=k,Z_2=k\right)\Pr\left(s_{PU}\neq s_{SU}\right)\\&=\frac{1}{4}\sum_{k=0}^{\infty}\Theta\left(k,\lambda_{PU}I_1+\lambda_b\right)\Theta\left(k,\lambda_{SU}I_2+\lambda_b\right)\end{aligned} \tag{42}$$

Case A-2: Same data sent

When the same data are sent, the two laser pulses overlap. However, the time slot without a signal is occupied by background radiation. The average number of photoelectrons in the two time slots are $\lambda_{PU}I_1+\lambda_{SU}I_2+\lambda_b$ and λ_b respectively. The conditional SEP of PU in this case can be evaluated as

$$\begin{aligned}P_s^{PU,A-2,BR}\left(e\,|\,I_1,I_2\right)&=\frac{1}{2}\sum_{k=0}^{\infty}\Pr\left(Z_1=k,Z_2=k\right)\Pr\left(s_{PU}=s_{SU}\right)\\&=\frac{1}{4}\sum_{k=0}^{\infty}\Theta\left(k,\lambda_{PU}I_1+\lambda_{SU}I_2+\lambda_b\right)\Theta\left(k,\lambda_b\right)\end{aligned} \tag{43}$$

Case B: Nonrandom decision

If $z_1\neq z_2$, wrong decisions are divided into the following two categories.

Case B-1: Different data sent

In this case the average numbers of photoelectrons in two slots are $\lambda_{PU}I_1+\lambda_b$ and $\lambda_{SU}I_2+\lambda_b$ respectively. If the time slot for SU data has more photoelectrons than that for PU data, the receiver will interpret it as the wrong data for PU. The conditional SEP for PU in this case can be written as

$$P_s^{PU,B-1,BR}\left(e\,|\,I_1,I_2\right)=\frac{1}{2}\sum_{i=1}^{\infty}\sum_{j=0}^{i-1}\Theta\left(i,\lambda_{SU}I_2+\lambda_b\right)\Theta\left(j,\lambda_{PU}I_1+\lambda_b\right) \tag{44}$$

Case B-2: Same data sent

The conditional SEP for PU in case B-2 can be obtained in the same way as in cases A-2 and B-1, *i.e.*

$$P_s^{PU,B-2,BR}\left(e\,|\,I_1,I_2\right)=\frac{1}{2}\sum_{i=1}^{\infty}\sum_{j=0}^{i-1}\Theta\left(i,\lambda_b\right)\Theta\left(j,\lambda_{PU}I_1+\lambda_{SU}I_2+\lambda_b\right) \tag{45}$$

Overall, the conditional SEP for PU in the background-radiation scenario is

$$\begin{aligned}P_s^{PU,BR}\left(e\,|\,I_1,I_2\right)=&\frac{1}{4}\sum_{k=0}^{\infty}\Big[\Theta\left(k,\lambda_{PU}I_1+\lambda_b\right)\Theta\left(k,\lambda_{SU}I_2+\lambda_b\right)\\&+\Theta\left(k,\lambda_{PU}I_1+\lambda_{SU}I_2+\lambda_b\right)\Theta\left(k,\lambda_b\right)\Big]\\&+\frac{1}{2}\sum_{i=1}^{\infty}\sum_{j=0}^{i-1}\Big[\Theta\left(i,\lambda_{SU}I_2+\lambda_b\right)\Theta\left(j,\lambda_{PU}I_1+\lambda_b\right)\\&+\Theta\left(i,\lambda_b\right)\Theta\left(j,\lambda_{PU}I_1+\lambda_{SU}I_2+\lambda_b\right)\Big]\end{aligned} \tag{46}$$

The average SEP of PU in the background-radiation scenario can be numerically evaluated, though its analytic expression is difficult to obtain. In the ideal no-fading condition I_1 and I_2 are assumed to be unity, and in the region of high symbol energy $\lambda_{PU}I_1+\lambda_{SU}I_2+\lambda_b$ is usually

large enough to guarantee that the items containing it in Eq. (46) go to zero. Thus the approximate expression for SEP of PU in this background-radiation-no-fading scenario is

$$P_s^{PU,Appro,BR} \approx \frac{1}{4}\sum_{k=0}^{\infty}\Theta\left(k,\lambda_{PU}+\lambda_b\right)\Theta\left(k,\lambda_{SU}+\lambda_b\right) + \frac{1}{2}\sum_{i=1}^{\infty}\sum_{j=0}^{i-1}\Theta\left(i,\lambda_{SU}+\lambda_b\right)\Theta\left(j,\lambda_{PU}+\lambda_b\right) \tag{47}$$

4.3. Symbol-error Probability of SU

In this section we derive the conditional SEP of SU in the background-radiation scenario. From Eq. (41), we know that wrong decisions for SU data occur in the following cases.

Case A: Random decision

The SEP for SU in this case is the same as the SEP for PU when $z_1 = z_2$, *i.e.*

$$P_s^{SU,A,BR}\left(e \mid I_1, I_2\right) = P_s^{PU,A-1,BR}\left(e \mid I_1, I_2\right) + P_s^{PU,A-2,BR}\left(e \mid I_1, I_2\right) \tag{48}$$

Case B: Nonrandom decision

If $z_1 \neq z_2$, we adopt the following expression to evaluate the conditional SEP for SU:

$$P_s^{SU,B,BR}\left(e \mid I_1, I_2\right) = \sum_{i=0}^{3} P\left(e \mid H_i, I_1, I_2\right) P\left(H_i\right) \tag{49}$$

where $P\left(e \mid H_i, I_1, I_2\right)$ is the error probability under hypothesis H_i conditioned on I_1 and I_2, and $P\left(H_i\right)$ is the prior probability of hypothesis H_i. In our FSO communication system, symbols 1 and 2 are transmitted with equal probability for both PU and SU. Hence the four hypotheses $H_i, i = 0,1,2,3$ are equally probable. The conditional SEP for SU in case B can be written as

$$P_s^{SU,B,BR}\left(e \mid I_1, I_2\right) = \frac{1}{4}\sum_{i=0}^{3} P\left(e \mid H_i, I_1, I_2\right) \tag{50}$$

Then we can derive the four conditional error probabilities $P\left(e \mid H_i, I_1, I_2\right), i = 0,1,2,3$ respectively.

First, we consider $P\left(e \mid H_0, I_1, I_2\right)$. Under hypothesis H_0, symbol 1 is sent by both PU and SU, and the laser pulses overlap in the first time slot. The photoelectron number in this time slot obeys the Poissonian distribution with parameter $\lambda_{PU} I_1 + \lambda_{SU} I_2 + \lambda_b$. Similarly, the second slot has $Z_2 \sim \pi\left(\lambda_b\right)$ photoelectrons. According to Eq. (41), if $1 < z_1 / z_2 < \kappa$ or $z_1 / z_2 < 1/\kappa$, the receiver will judge SU data as symbol 2, and the wrong decision occurs. The conditional error probability under hypothesis H_0 can be expressed as

$$P\left(e \mid H_0, I_1, I_2\right) = \left[\sum_{i=1}^{\infty}\sum_{j=0}^{i-1}\Theta\left(i,\lambda_{PU}I_1+\lambda_{SU}I_2+\lambda_b\right)\Theta\left(j,\lambda_b\right)\right] \times \left[\sum_{i=1}^{\infty}\sum_{j=0}^{J_1}\Theta\left(i,\lambda_b\right)\Theta\left(j,\lambda_{PU}I_1+\lambda_{SU}I_2+\lambda_b\right)\right] + \left[\sum_{i=1}^{\infty}\sum_{j=0}^{J_2}\Theta\left(i,\lambda_b\right)\Theta\left(j,\lambda_{PU}I_1+\lambda_{SU}I_2+\lambda_b\right)\right] \tag{51}$$

where J_1 and J_2 are two integers defined as $J_1 = \lfloor \kappa i \rfloor$ and $J_2 = \lfloor i/\kappa \rfloor$.

Second, under hypothesis H_1 symbols 1 and 2 are sent by PU and SU respectively. Then $Z_1 \sim \pi\left(\lambda_{PU} I_1 + \lambda_b\right)$ and $Z_2 \sim \pi\left(\lambda_{SU} I_2 + \lambda_b\right)$. If $z_1 / z_2 > \kappa$ or $1/\kappa < z_1 / z_2 < 1$, the receiver will decide SU data to be symbol 1, which is also wrong. Therefore, $P\left(e \mid H_1, I_1, I_2\right)$ is

$$P\left(e \mid H_1, I_1, I_2\right) = \left[\sum_{i=1}^{\infty}\sum_{j=0}^{i-1}\Theta\left(i,\lambda_{SU}I_2+\lambda_b\right)\Theta\left(j,\lambda_{PU}I_1+\lambda_b\right)\right] \times \left[\sum_{i=1}^{\infty}\sum_{j=0}^{J_1}\Theta\left(i,\lambda_{PU}I_1+\lambda_b\right)\Theta\left(j,\lambda_{SU}I_2+\lambda_b\right)\right] + \left[\sum_{i=1}^{\infty}\sum_{j=0}^{J_2}\Theta\left(i,\lambda_{PU}I_1+\lambda_b\right)\Theta\left(j,\lambda_{SU}I_2+\lambda_b\right)\right] \tag{52}$$

Due to the symmetry of the decision rule in Eq. (41), the conditional error probability under H_2 is equal to that under H_1, namely $P\left(e \mid H_1, I_1, I_2\right) = P\left(e \mid H_2, I_1, I_2\right)$. Similarly, this symmetry also holds for H_0 and H_3, *i.e.* $P\left(e \mid H_0, I_1, I_2\right) = P\left(e \mid H_3, I_1, I_2\right)$.

Finally, substituting Eqs. (48), (51), and (52) into $P_s^{SU,BR} = P_s^{SU,A,BR} + P_s^{SU,B,BR}$, we can obtain the conditional SEP expression for SU in the background-radiation scenario as

$$\begin{aligned} P_s^{SU,BR}\left(e \mid I_1, I_2\right) = {} & \frac{1}{4}\sum_{k=0}^{\infty}\left[\Theta\left(k,\lambda_{PU}I_1+\lambda_b\right)\Theta\left(k,\lambda_{SU}I_2+\lambda_b\right) + \Theta\left(k,\lambda_{PU}I_1+\lambda_{SU}I_2+\lambda_b\right)\Theta\left(k,\lambda_b\right)\right] \\ & + \frac{1}{2}\left\{\left[\sum_{i=1}^{\infty}\sum_{j=0}^{i-1}\Theta\left(i,\lambda_{PU}I_1+\lambda_{SU}I_2+\lambda_b\right)\Theta\left(j,\lambda_b\right)\right]\left[\sum_{i=1}^{\infty}\sum_{j=0}^{J_1}\Theta\left(i,\lambda_b\right)\Theta\left(j,\lambda_{PU}I_1+\lambda_{SU}I_2+\lambda_b\right)\right]\right. \\ & + \left[\sum_{i=1}^{\infty}\sum_{j=0}^{i-1}\Theta\left(i,\lambda_{SU}I_2+\lambda_b\right)\Theta\left(j,\lambda_{PU}I_1+\lambda_b\right)\right]\left[\sum_{i=1}^{\infty}\sum_{j=0}^{J_1}\Theta\left(i,\lambda_{PU}I_1+\lambda_b\right)\Theta\left(j,\lambda_{SU}I_2+\lambda_b\right)\right] \\ & \left. + \sum_{i=1}^{\infty}\sum_{j=0}^{J_2}\left[\Theta\left(i,\lambda_b\right)\Theta\left(j,\lambda_{PU}I_1+\lambda_{SU}I_2+\lambda_b\right) + \Theta\left(i,\lambda_{PU}I_1+\lambda_b\right)\Theta\left(j,\lambda_{SU}I_2+\lambda_b\right)\right]\right\} \end{aligned} \tag{53}$$

In no-fading channels $I_1 = I_2 = 1$, and $\lambda_{PU} + \lambda_{SU} + \lambda_b$ can be large enough to guarantee the items containing it in Eq. (53) approach zero in the high-symbol-energy region. Corresponding to the no-background-radiation scenario, the approximate SEP of SU in the background-radiation-no-fading scenario can also be obtained according to α. If $\alpha \to 1$, few decision errors occur in the random-decision case, and $P_s^{SU,A,BR}(e \mid I_1, I_2)$ approaches zero, while $\sum_{i=1}^{\infty}\sum_{j=0}^{i-1}\Theta(i, \lambda_{SU} + \lambda_b)\Theta(j, \lambda_{PU} + \lambda_b)$ approaches one. Then Eq. (53) can be approximated by

$$P_s^{SU,Appro} \approx \frac{1}{2}\left[\sum_{i=1}^{\infty}\sum_{j=0}^{J_1}\Theta(i, \lambda_b)\Theta(j, \lambda_{PU} + \lambda_{SU} + \lambda_b) + \sum_{i=1}^{\infty}\sum_{j=0}^{J_2}\Theta(i, \lambda_{PU} + \lambda_b)\Theta(j, \lambda_{SU} + \lambda_b)\right] \tag{54}$$

If $\alpha \to 0.5$, the power difference between PU and SU is small, and the approximate expression is

$$\begin{aligned} P_s^{SU,Appro} \approx{}& \frac{1}{4}\sum_{k=0}^{\infty}\left[\Theta(k, \lambda_{PU} + \lambda_b)\Theta(k, \lambda_{SU} + \lambda_b) + \Theta(k, \lambda_{PU} + \lambda_{SU} + \lambda_b)\Theta(k, \lambda_b)\right] \\ &+ \frac{1}{2}\left\{\left[\sum_{i=1}^{\infty}\sum_{j=0}^{i-1}\Theta(i, \lambda_{SU} + \lambda_b)\Theta(j, \lambda_{PU} + \lambda_b)\right]\left[\sum_{i=1}^{\infty}\sum_{j=0}^{J_1}\Theta(i, \lambda_{PU} + \lambda_b)\Theta(j, \lambda_{SU} + \lambda_b)\right]\right. \\ &\left. + \sum_{i=1}^{\infty}\sum_{j=0}^{J_2}\left[\Theta(i, \lambda_b)\Theta(j, \lambda_{PU} + \lambda_{SU} + \lambda_b) + \Theta(i, \lambda_{PU} + \lambda_b)\Theta(j, \lambda_{SU} + \lambda_b)\right]\right\} \end{aligned} \tag{55}$$

V. RESULTS

In this section we present numerical simulation results for the SEP of PU and SU, with and without background radiation. In the no-background-radiation scenario, both the conditional SEP in the ideal no-fading channel and the average SEP in the practical channel with atmospheric turbulence are evaluated, while in the background-radiation scenario, only the conditional SEP is discussed. In our simulations the laser sources are assumed to be 1500 nm in wavelength, and the quantum efficiency η is unity.

5.1. Numerical Simulations without Background Radiation

The conditional SEP performance of PU without background radiation is shown in Fig. 3. The simulation is conducted in an ideal no-fading channel, *i.e.* $I_1 = I_2 = 1$. The horizontal axis represents the total symbol energy, and the four curves correspond to different values of the power ratio α. For one curve with exact power ratio, we can see that the SEP of PU decreases as the total symbol energy increases. In addition, if we fix the total symbol energy we can observe that the SEP performance of PU deteriorates with decreasing α. In an FSO system with fixed total power, decreasing α means SU has larger transmitted power. As mentioned above, the pulses sent by SU can be treated as interference with PU in the decision; hence decrease in α can deteriorate PU performance.

Figure 4 depicts the conditional SEP of SU in the no-background-radiation and no-fading scenario. For a better understanding, we illustrate the SEP of SU in three-dimensional coordinates. The *x*-axis represents total symbol energy and the *y*-axis is the power ratio α, varying from 0.6 to 1. The *z*-axis represents the SEP of SU, in log scale. In Fig. 4 we can clearly see that this SEP decreases with increasing total symbol energy, which is the same as the case for PU. However, the SEP of SU is no longer a monotonic function of α. If we fix the total symbol energy and vary α from 0.6 to 1, this SEP decreases at

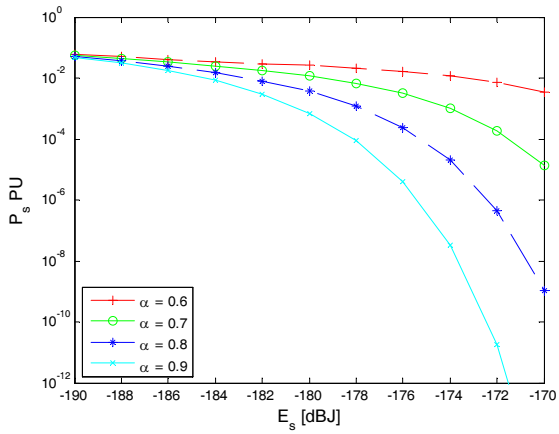

FIG. 3. Conditional SEP of PU without background radiation, when $I_1 = I_2 = 1$.

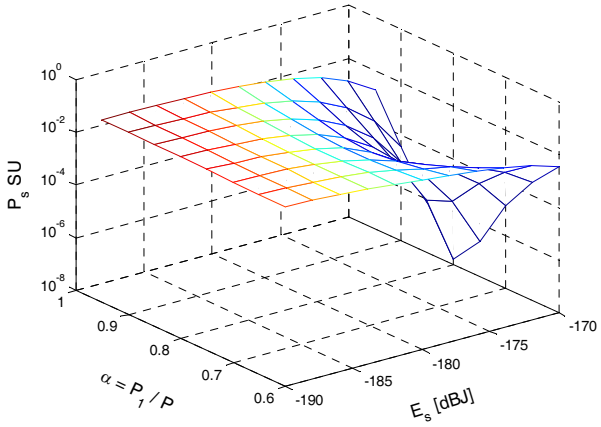

FIG. 4. Conditional SEP of SU without background radiation, when $I_1 = I_2 = 1$.

first, then increases. Moreover, as E_s increases, this fall and rise of the SEP becomes more and more obvious. We can explain this interesting phenomenon in the following aspects: First, when α increases from 0.5 to the optimum point, the power of PU increases and less power is allocated to SU. Therefore, the difference in photoelectron number between PU and SU increases, which means that the error probability in the random-decision cases is reduced, while in the nonrandom-decision case SU is less likely to have more photoelectrons than PU. Consequently, the SEP of SU decreases at this stage. Second, when α increases further from the optimum point to 1, SU has less and less power, and the average photoelectron number of the SU pulse decreases. If PU sends different data than SU and the time slot for SU is empty, SU will be considered as sending the same data as PU, which actually is wrong, and the probability of this incorrect decision increases in the second stage, so that the SEP of SU rises.

Figure 5 presents the approximate SEP performance of PU and SU in the no-background-radiation and no-fading scenario. In Fig. 5(a) the solid curves give the exact SEP of PU using Eq. (15), in which I_1 and I_2 are set to 1, and the dotted curves are obtained from the approximate expression for SEP of PU in Eq. (23). We evaluate the exact and approximate expressions for SEP of PU for different values of the power ratio, $\alpha = 0.7$ and $\alpha = 0.9$. We find that when the total symbol energy is larger than -180 dB J, the curves in Fig. 5(a) show the tightness of this approximation. Similar simulations for SU are also presented in Fig. 5(b). The exact curves are evaluated using Eq. (28), and the approximate curves are plotted according to α. For $\alpha = 0.6$ we use Eq. (30a) to evaluate the SEP of SU, and for $\alpha = 0.9$ we use Eq. (30b). We can see that the curves in Fig. 5(b) also converge to the exact result in the high-symbol-energy region.

The average SEP of PU and SU in channels with fading due to atmospheric turbulence and misalignment are shown in Figure 6. The channel parameters are chosen as follows: $\sigma_x^2 = 1.5$ represents medium turbulence, $\omega_z / r = 6$ represents normalized beam width, and $\sigma_s / r = 1$ denotes normalized

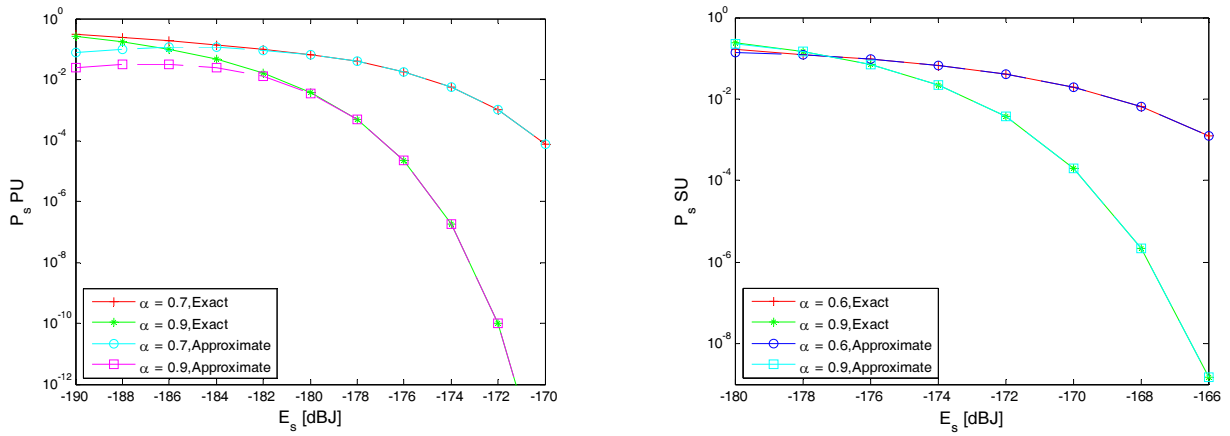

(a) (b)

FIG. 5. Approximate SEP without background radiation, when $I_1 = I_2 = 1$: (a) approximate SEP of PU; (b) approximate SEP of SU.

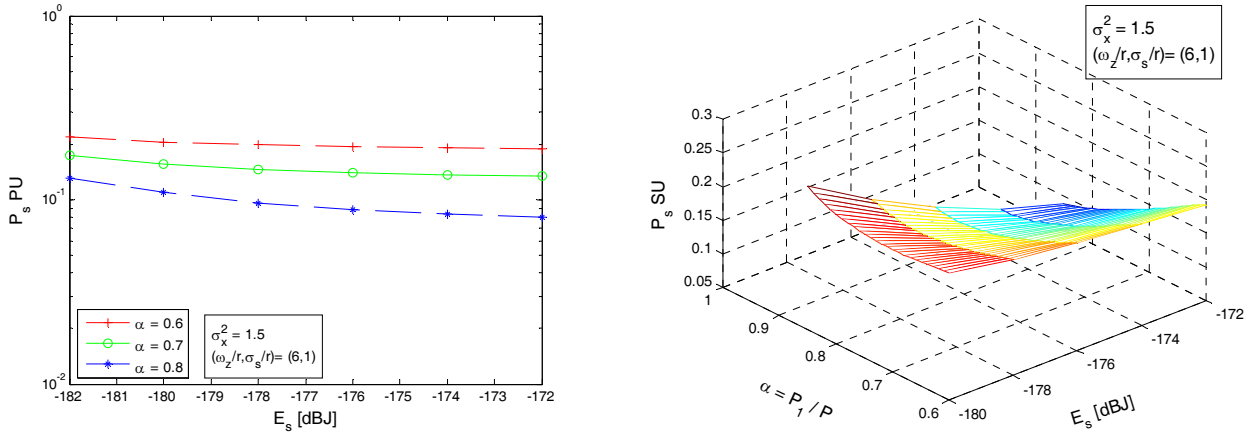

(a) (b)

FIG. 6. Average SEP in fading channels without background radiation: (a) average SEP of PU; (b) average SEP of SU.

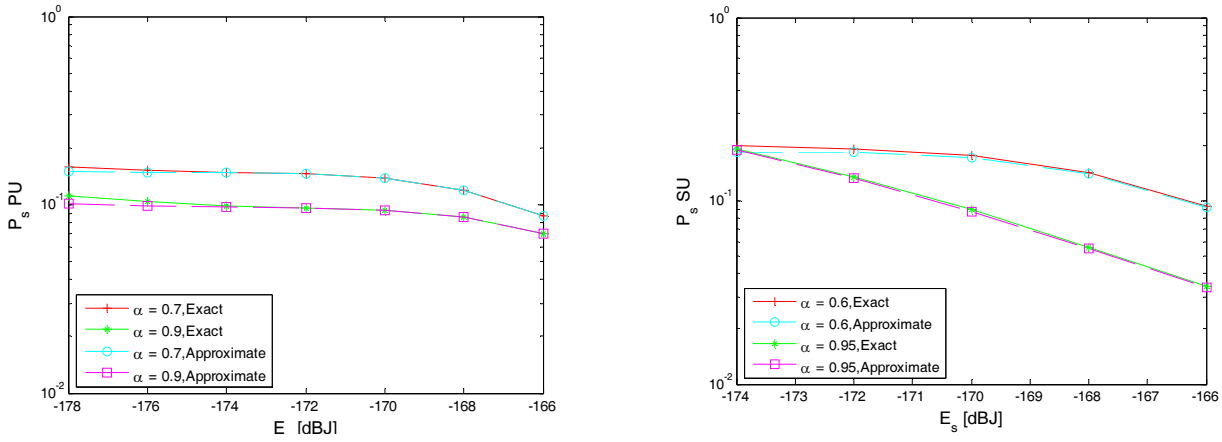

FIG. 7. Approximate average SEP of PU and SU without background radiation: (a) average SEP of PU; (b) average SEP of SU.

jitter at the receiver. The SEP curves are derived with different symbol energies and different power ratios. Comparing the curves in Fig. 6 to those in Figs. 3 and 4, we can draw similar conclusions, *i.e.* the SEP decreases with increasing symbol energy. Although the SEP of PU and SU in the fading channels are much larger than that in the ideal channels, the power ratio plays a similar role in SEP performance. For PU, larger power ratio means better communication quality. For SU, an optimal power ratio exists to ensure that the SEP of SU reaches its lowest point.

The approximate average SEP of PU and SU in channels with fading due to atmospheric turbulence and misalignment is shown in Fig. 7. We use the same channel parameters as in Fig. 6. In Fig. 7(a) the exact SEP curves of PU coincide with the approximate curves, which verifies Eq. (24). In Fig. 7(b) we take $\alpha = 0.6$ to represent $\alpha \to 0.5$, and the approximate simulation result is calculated using Eq. (31a). Similarly, we use $\alpha = 0.95$ to represent $\alpha \to 1$, and Eq. (31b) is adopted. The curves in Fig. 7(b) verify the approximate average SEP expressions in Eq. (31).

5.2. Numerical Simulations with Background Radiation

Now we take background radiation into consideration. The simulation parameters are the same as the previous ones in the no-background-radiation section, *i.e.* $I_1 = I_2 = 1$. Figure 8 demonstrates the SEP curves of PU in the background-radiation scenario. We take the background radiation energy for each time slot as -195 dB J. In Fig. 8, the horizontal axis denotes the total symbol energy of PU and SU. These results yield similar conclusions as in the no-background-radiation scenario. The communication performance of PU can be improved by either increasing total transmitted power or α.

To further study the influence of background radiation on PU communication performance, we simulate the conditional SEP of PU for different background-radiation powers in Fig. 9. Comparing the two groups of parallel curves, we can see that for a given α, the SEP performance of PU deteriorates with increasing background radiation. Furthermore, this deterioration becomes more serious if we increase

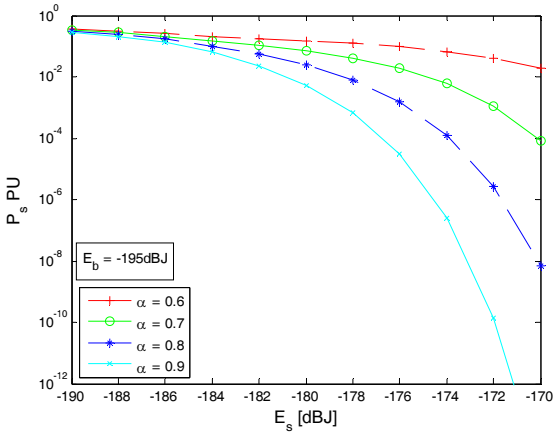

FIG. 8. Conditional SEP of PU with background radiation, when $I_1 = I_2 = 1$.

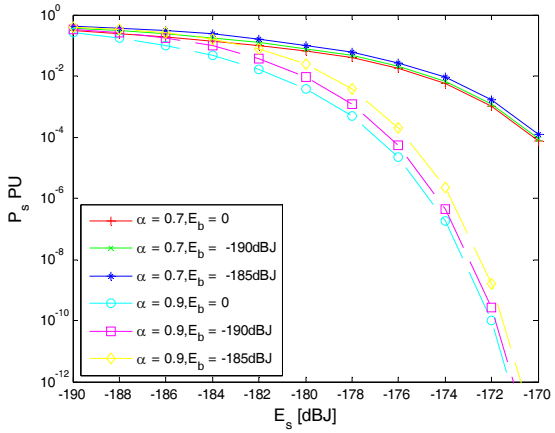

FIG. 9. Conditional SEP of PU under different levels of background radiation, when $I_1 = I_2 = 1$.

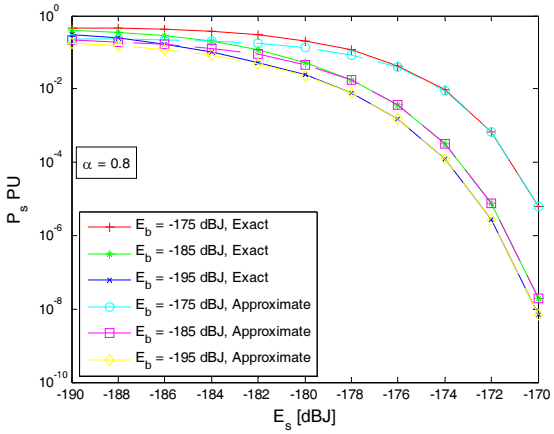

FIG. 10. Approximate SEP of PU with background radiation, when $I_1 = I_2 = 1$.

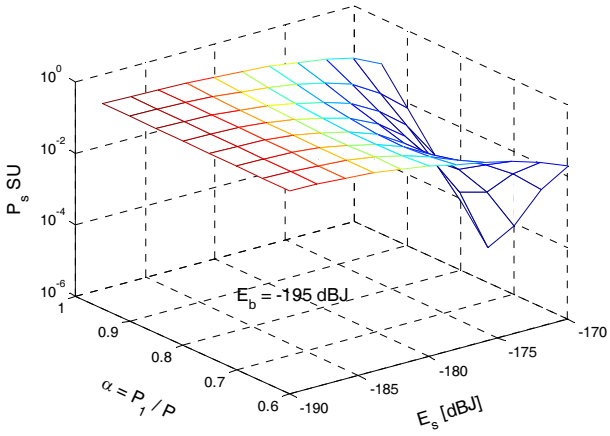

FIG. 11. Conditional SEP of SU with background radiation, when $I_1 = I_2 = 1$.

the power ratio: If we increase α, the transmitted power of SU decreases. For PU, both SU and background radiation can be treated as interference. A higher power ratio means that background radiation plays a more important part in this interference; hence, it has more effect on the performance of PU.

In Fig. 10 we illustrate the approximate SEP performance of PU with different background-radiation energies, using the exact expression of Eq. (46) and the approximate expression of Eq. (47) respectively. Three groups of curves show the tightness of this approximation. Moreover, when we take $\alpha = 0.8$ and gradually increase background-radiation energy from -195 dB J to -175 dB J, the approximation becomes worse. Since the approximate SEP expression of PU is obtained by ignoring items with $\lambda_{PU} + \lambda_{SU} + \lambda_b$, the increase of background radiation will make the ignored items have more impact on the overall SEP performance. Therefore, increase in background radiation deteriorates the fidelity of the approximation.

The conditional SEP performance of SU with background radiation is provided in Fig. 11. As for the simulations in the no-background-radiation scenario, these results are presented in three-dimensional coordinates, per Fig. 4. We fix the background radiation energy E_b at -195 dB J in the simulation. From this figure, we find that SU can achieve better communication performance with increase of total transmitted power. If we fix the total symbol energy and change the power ratio, there will be an optimal point at which SU performs best. This phenomenon can be explained using the analysis of Fig. 4.

Finally, Fig. 12 presents the approximate SEP performance of SU under different background-radiation energies. In Fig. 12(a) the power ratio is 0.9, corresponding to $\alpha \to 1$, and the approximate expression of Eq. (54) is adopted to obtain the curves. In Fig. 12(b) $\alpha = 0.6$, and the approximate SEP is evaluated using Eq. (55). All curves in Fig. 12 show the tightness of the approximation. Furthermore, in Fig. 12(b), we also find that the curves with lower background-radiation energy achieve better performance of the approximation.

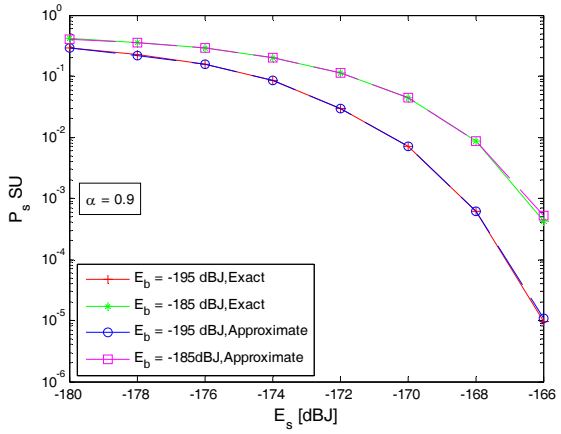

(a)

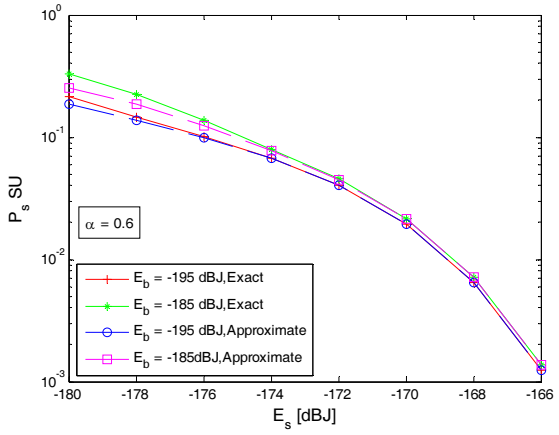

(b)

FIG. 12. Approximate SEP of SU with different levels of background radiation, when $I_1 = I_2 = 1$: (a) $\alpha = 0.9$; (b) $\alpha = 0.6$.

VI. CONCLUSION

This paper considers a two-user free-space optical (FSO) communication system with a shared detector. We investigate the performance of this system in the absence and presence of background radiation. Exact and approximate SEP expressions for the two users are derived. Numerical simulations are presented, and the results demonstrate that both PU and SU can achieve better communication performance as the total transmitted power increases. Both atmospheric turbulence and misalignment errors can deteriorate PU and SU SEP performance. In an ideal no-fading channel, we find that the SEP of PU decreases monotonically with increasing power ratio; hence we can say that the more power distributed to PU, the better performance PU achieves. However, this is not true for SU: Interestingly, there is an optimal power ratio for which SU achieves minimum SEP. We also demonstrate that background radiation deteriorates the performance of PU, and this deterioration is particularly obvious in the region of high power ratio. At last, the simulation results also show the high fidelity of our SEP approximation, which is useful and necessary for the performance analysis of this FSO communication system.

VII. APPENDIX

Appendix: Proof of Eq. (38)

In this appendix we prove that Eq. (38) holds. First, we derive the condition for the following inequality:

$$\frac{\ln\left(1+\lambda_{SU}I_2/\lambda_b\right)}{\ln\left[1+\lambda_{SU}I_2/\left(\lambda_{PU}I_1+\lambda_b\right)\right]} > \frac{\ln\left(1+\lambda_{PU}I_1/\lambda_b\right)}{\ln\left[1+\lambda_{PU}I_1/\left(\lambda_{SU}I_2+\lambda_b\right)\right]} \tag{A.1}$$

(A.1) is equivalent to

$$\begin{aligned}&\left[\ln\left(\lambda_{SU}I_2+\lambda_b\right)-\ln\left(\lambda_b\right)\right]\times\\&\left[\ln\left(\lambda_{PU}I_1+\lambda_{SU}I_2+\lambda_b\right)-\ln\left(I_2\lambda_{SU}+\lambda_b\right)\right]>\\&\left[\ln\left(\lambda_{PU}I_1+\lambda_b\right)-\ln\left(\lambda_b\right)\right]\times\\&\left[\ln\left(\lambda_{PU}I_1+\lambda_{SU}I_2+\lambda_b\right)-\ln\left(\lambda_{PU}I_1+\lambda_b\right)\right]\end{aligned} \tag{A.2}$$

Further expanding (A.2) and eliminating common item $\ln\lambda_b \ln\left(\lambda_{PU}I_1+\lambda_{SU}I_2+\lambda_b\right)$, we have

$$\begin{aligned}&\ln\left(\lambda_{SU}I_2+\lambda_b\right)\ln\left(\lambda_{PU}I_1+\lambda_{SU}I_2+\lambda_b\right)-\\&\left[\ln\left(\lambda_{SU}I_2+\lambda_b\right)\right]^2+\ln\lambda_b\ln\left(\lambda_{SU}I_2+\lambda_b\right)>\\&\ln\left(\lambda_{PU}I_1+\lambda_b\right)\ln\left(\lambda_{PU}I_1+\lambda_{SU}I_2+\lambda_b\right)-\\&\left[\ln\left(\lambda_{PU}I_1+\lambda_b\right)\right]^2+\ln\lambda_b\ln\left(\lambda_{PU}I_1+\lambda_b\right)\end{aligned} \tag{A.3}$$

Shifting the items on the right side of (A.3) and combining the common items, (A.3) becomes

$$\begin{aligned}\ln\frac{\lambda_{SU}I_2+\lambda_b}{\lambda_{PU}I_1+\lambda_b}\times\Big[&\ln\left(\lambda_{PU}I_1+\lambda_{SU}I_2+\lambda_b\right)\\&-\ln\left[\left(\lambda_{PU}I_1+\lambda_b\right)\left(\lambda_{SU}I_2+\lambda_b\right)\right]+\ln\lambda_b\Big]>0\end{aligned} \tag{A.4}$$

$\ln\left(\lambda_{PU}I_1+\lambda_{SU}I_2+\lambda_b\right)-\ln\left[\left(\lambda_{PU}I_1+\lambda_b\right)\left(\lambda_{SU}I_2+\lambda_b\right)\right]+\ln\lambda_b$ in the expression above can be written as $\ln\frac{\left(\lambda_{PU}I_1+\lambda_{SU}I_2+\lambda_b\right)\lambda_b}{\left(\lambda_{PU}I_1+\lambda_b\right)\left(\lambda_{SU}I_2+\lambda_b\right)}$, which in fact is negative. Then (A.1) holds when $\ln\frac{\lambda_{SU}I_2+\lambda_b}{\lambda_{PU}I_1+\lambda_b}$ is also negative, which is equivalent to $\lambda_{PU}I_1>\lambda_{SU}I_2$.

Similarly,

$$\frac{\ln\left(1+\lambda_{SU}I_2/\lambda_b\right)}{\ln\left[1+\lambda_{SU}I_2/\left(\lambda_{PU}I_1+\lambda_b\right)\right]}<\frac{\ln\left(1+\lambda_{PU}I_1/\lambda_b\right)}{\ln\left[1+\lambda_{PU}I_1/\left(\lambda_{SU}I_2+\lambda_b\right)\right]}$$

holds when $\lambda_{PU}I_1<\lambda_{SU}I_2$. Finally,

$$\kappa=\begin{cases}\dfrac{\ln\left(1+\lambda_{SU}I_2/\lambda_b\right)}{\ln\left[1+\lambda_{SU}I_2/\left(\lambda_{PU}I_1+\lambda_b\right)\right]}, & \lambda_{PU}I_1\geq\lambda_{SU}I_2\\[2ex]\dfrac{\ln\left(1+\lambda_{PU}I_1/\lambda_b\right)}{\ln\left[1+\lambda_{PU}I_1/\left(\lambda_{SU}I_2+\lambda_b\right)\right]}, & \lambda_{PU}I_1<\lambda_{SU}I_2\end{cases}, \tag{A.5}$$

Thus Eq. (38) holds.

REFERENCES

1. M. A. Khalighi and M. Uysal, "Survey on free space optical communication: a communication theory perspective," IEEE Commun. Surveys Tuts. **16**, 2231-2258 (2014).
2. S. Arnon, M. Uysal, Z. Ghassemlooy, Z. Y. Xu, and J. L. Cheng, "Guest editorial optical wireless communications," IEEE J. Sel. Areas Commun. **33**, 1733-1737 (2015).
3. A. A. Farid and S. Hranilovic, "Outage capacity optimization for free-space optical links with pointing errors," J. Lightwave Technol. **25**, 1702-1710 (2007).
4. M.-A. Khalighi, N. Schwartz, N. Aitamer, and S. Bourennane, "Fading reduction by aperture averaging and spatial diversity in optical wireless systems," J. Opt. Commun. Netw. **1**, 580 (2009).
5. L. C. Andrews, "Aperture-averaging factor for optical scintillations of plane and spherical waves in the atmosphere," J. Opt. Soc. Am. A, **9**, 597 (1992).
6. E. J. Lee and V. W. S. Chan, "Part 1: Optical communication over the clear turbulent atmospheric channel using diversity," IEEE J. Sel. Areas Commun. **22**, 1896-1906 (2004).
7. S. M. Navidpour, M. Uysal, and M. Kavehrad, "BER performance of free-space optical transmission with spatial diversity," IEEE Trans. Wireless Commun. **6**, 2813-2819 (2007).
8. A. Garcia-Zambrana, C. Castillo-Vazquez, and B. Castillo-

Vazquez, "Space-time trellis coding with transmit laser selection for FSO links over strong atmospheric turbulence channels," Opt. Express **18**, 5356-5366 (2010).
9. J. A. Anguita, M. A. Neifeld, and B. V. Vasic, "Spatial correlation and irradiance statistics in a multiple-beam terrestrial free-space optical communication link," Appl. Opt. **46**, 6561-6571 (2007).
10. S. G. Wilson, M. Brandt-Pearce, Q. L. Cao, and J. H. Leveque, "Free-space optical MIMO transmission with Q-ary PPM," IEEE Trans. Commun. **53**, 1402-1412 (2005).
11. S. G. Wilson, M. Brandt-Pearce, Q. L. Cao, and M. Baedke, "Optical repetition MIMO transmission with multipulse PPM," IEEE J. Sel. Areas Commun. **23**, 1901-1910 (2005).
12. T. A. Tsiftsis, H. G. Sandalidis, G. K. Karagiannidis, and M. Uysal, "Optical wireless links with spatial diversity over strong atmospheric turbulence channels," IEEE Trans. Wireless Commun. **8**, 951-957 (2009).
13. M. R. Bhatnagar and Z. Ghassemlooy, "Performance analysis of Gamma-Gamma fading FSO MIMO links with pointing errors," J. Lightwave Technol. **34**, 2158-2169 (2016).
14. J. Zhang, L. Dai, Y. Han, Y. Zhang, and Z. Wang, "On the ergodic capacity of MIMO free-space optical systems over turbulence channels," IEEE J. Sel. Areas Commun. **33**, 1925-1934 (2015).
15. A. A. Farid and S. Hranilovic, "Diversity gain and outage probability for MIMO free-space optical links with misalignment," IEEE Trans. Commun. **60**, 479-487 (2012).
16. A. Garcia-Zambrana, C. Castillo-Vazquez, and B. Castillo-Vazquez, "Outage performance of MIMO FSO links over strong turbulence and misalignment fading channels," Opt. Express **19**, 13480-13496 (2011).
17. N. Letzepis and A. G. I. Fabregas, "Outage probability of the gaussian MIMO free-space optical channel with PPM," IEEE Trans. Commun. **57**, 3682-3690 (2009).
18. I. B. Djordjevic, "Adaptive modulation and coding for free-space optical channels," J. Opt. Commun. Netw. **2**, 221-229 (2010).
19. O. Barsimantov and V. V. Nikulin, "Adaptive optimization of a free space laser communication system under dynamic link attenuation," J. Opt. Commun. Netw. **3**, 215-222 (2011).
20. A. Garcia-Zambrana, C. Castillo-Vazquez, B. Castillo-Vazquez, and R. Boluda-Ruiz, "Bit detect and forward relaying for FSO links using equal gain combining over gamma-gamma atmospheric turbulence channels with pointing errors," Opt. Express **20**, 16394-16409 (2012).
21. R. Boluda-Ruiz, A. Garcia-Zambrana, C. Castillo-Vazquez, and B. Castillo-Vazquez, "Adaptive selective relaying in cooperative free-space optical systems over atmospheric turbulence and misalignment fading channels," Opt. Express **22**, 16629-16644 (2014).
22. C. Abou-Rjeily and A. Slim, "Cooperative diversity for free-space optical communications: transceiver design and performance analysis," IEEE Trans. Commun. **59**, 658-663 (2011).
23. N. D. Chatzidiamantis, L. Georgiadis, H. G. Sandalidis, and G. K. Karagiannidis, "Throughput-optimal link-layer design in power constrained hybrid OW/RF systems," IEEE J. Sel. Areas Commun. **33**, 1972-1984 (2015).
24. Y. Tang and M. Brandt-Pearce, "Link allocation, routing, and scheduling for hybrid FSO/RF wireless mesh networks," J. Opt. Commun. Netw. **6**, 86-95 (2014).
25. F. Yang, J. L. Cheng, and T. A. Tsiftsis, "Free-space optical communication with nonzero boresight pointing errors," IEEE Trans. Commun. **62**, 713-725 (2014).
26. W. P. Z. Ghassemlooy and S. Rajbhandari, *Optical wireless communications system and channel modelling with MATLAB.* (CRC Press, Boca Raton, 2013).
27. C. Abou-Rjeily and S. Haddad, "Inter-relay cooperation: a new paradigm for enhanced relay-assisted FSO communications," IEEE Trans. Commun. **62**, 1970-1982 (2014).
28. A. Mostafa and S. Hranilovic, "Channel measurement and markov modeling of an urban free-space optical link," J. Opt. Commun. Netw. **4**, 836-846 (2012).
29. A. Papoulis and S. U. Pillai, Probability, *Random variables and stochastic processes*. (McGraw-Hill Companies, New York, 2002).
30. V. S. Adamchik and O. I. Marichev, "The algorithm for calculating integrals of hypergeometric type functions and its realization in REDUCE system," in *International Symposium on Symbolic and Algebraic Computation*, pp. 212-224 (1990).
31. http://functions.wolfram.com/HypergeometricFunctions/MeijerG/. (2015).